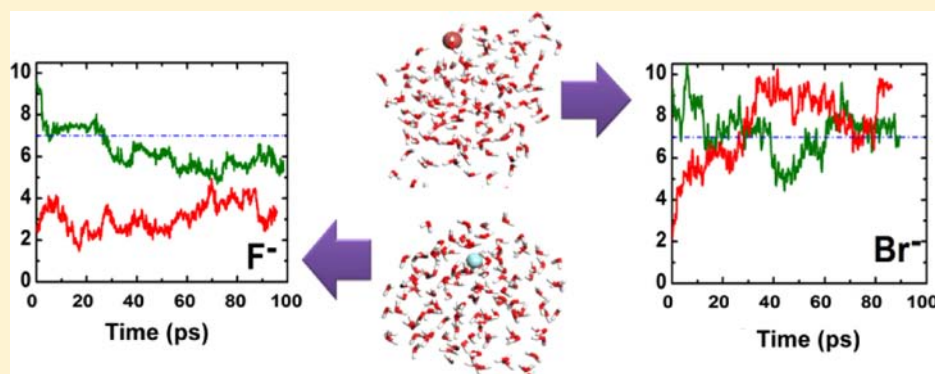


First-Principles Molecular Dynamics Simulation of Atmospherically Relevant Anion Solvation in Supercooled Water Droplet

Yu Zhao, Hui Li, and Xiao Cheng Zeng*

Department of Chemistry, University of Nebraska-Lincoln, Lincoln, Nebraska 68588, United States

S Supporting Information



ABSTRACT: We present a comprehensive first-principles Born–Oppenheimer molecular dynamics (BOMD) simulation study of halide anion solvation in a deeply supercooled water droplet (with diameter ~ 1.8 nm). We show that larger halide anions Br^- and I^- show “outer-layer surface preference”, whereas F^- exhibits bulk preference. Contrary to behavior of other halide anions, Cl^- in the water droplet appears to exhibit no strong tendency of surface or bulk preference at either the supercooled or ambient condition, a phenomenon not previously reported in the literature. BOMD simulation indicates that fully hydrated complex of F^- is mainly five-fold coordinated (showing square pyramid structure), whereas Cl^- , Br^- and I^- hydrated complexes are either five- or six-fold coordinated (showing sandwich-like structure). Among Cl^- , Br^- and I^- anions, BOMD simulation indicates that I^- exhibits the largest diffusion coefficient despite its largest size. However, computed resident time of the four halide ions suggests that Br^- can approach from the interior to the surface of the water droplet at a much faster rate than I^- and Cl^- .

INTRODUCTION

Propensity of ionic species at the air–water interface can play a key role in the uptake and chemical reactions of gases with liquid droplets in the lower troposphere (particularly, the marine boundary layer). Previous surface-sensitive spectroscopy measurements and classical molecular dynamics (MD) simulations have demonstrated that at room temperature halide anions Cl^- , Br^- , and I^- prefer to be at the surface of water (surface preference), whereas the smallest halide anion F^- tends to be fully solvated inside water (bulk preference).^{1–14} However, few studies have been reported on the process of halide ions in supercooled water droplets (e.g., with temperature from -1 to -50 °C, a typical temperature range in troposphere at midlatitudes). A better understanding of propensity of ions toward the air–water interface has important implications for processes in atmospheric chemistry, such as the ozone cycle below the room temperature,^{1–8} and in biochemistry, such as the different ability of ions to precipitate or denature protein at or below the room temperature.⁹ For example, the ozone depletion on Antarctica is largely attributed to reactive halogen species (e.g., Br and BrO), which are yielded through photochemistry from inert halide salt ions (e.g., Br^-).^{15–20} Typically, the oxidation of halide anions occurs

much faster at the interface than in the bulk solution.²¹ In the lower troposphere, such air–water interfaces may play a larger role in the uptake and reaction of gases (e.g., O_3) with different kinetics and mechanisms from those in bulk solutions.²² Hence, the behavior of halides near air–water interfaces has attracted considerable interests.

At first sight, the notion of the surface enhancement of halide concentrations appears to be against physics, as electrostatic image forces would repel ions away from the interfacial region and give minimized surface tension.²³ However, both experimental and theoretical investigations have shown higher concentrations of Cl^- , Br^- , and I^- in the interfacial region at the room temperature, compared to the bulk, whereas F^- is fully solvated in the interior of water.^{1–14} In previous experiments, detections were made via several state-of-the-art surface-sensitive techniques. Vibrational sum-frequency generation (VSFG) with Raman or IR spectroscopies suggests that the hydrogen-bonding network of water in the interfacial region for Br^- and I^- aqueous solution was distorted compared to the air–neat water interface, due to higher concentration of Br^-

Received: July 16, 2013

Published: September 23, 2013

and Γ^- near the surface.^{9,12} Ambient pressure X-ray photoelectron spectroscopy studies also support concentration enhancement of halide anions on deliquesced salt surfaces, except for F^- , and verify the larger, more polarizable halide anions can exhibit more surface enhancement.^{1,5–7} The same results were obtained from electrospray ionization mass spectrometry of salt solution⁴ and second harmonic generation spectroscopy (SHG) experiments.^{10,11} In addition to experimental studies, the accumulating behavior, structural characteristics, and charge distribution on the liquid–vapor interface of salt solution have also been investigated by many researchers using classical MD simulations based on nonpolarizable and polarizable water models.^{3,8,13,14} Recently, the free-energy profiles of halide anion solvation in water droplet have been computed based on molecular simulation,³ which show that the surface preference of Cl^- , Br^- , and I^- ions is mainly due to more favorable water–water interaction in the enthalpic component, whereas the interior preference of F^- is mainly due to entropic contribution. However, this conclusion still remains controversial.²⁴

Although the polarizability effects have been recognized in previous classical molecular simulations, recent theoretical investigations suggest that the ion dipole magnitude could be overestimated in simulations with undamped polarizable models.^{25–28} In addition, compared to the bulk, slightly decreased water dipole moments near halide ions are identified in density functional theory (DFT) interaction potentials.^{29,30} Several models for halide ions and water have been developed to avert such an overestimation.^{27,31–33} Despite of numerous results obtained from classical MD simulations, more accurate DFT-based first-principles MD simulations would be desirable in describing complex charge rearrangement and polarization and many-body effects as well as in providing benchmark results for the development of more accurate water/ion force fields. Toward this end, we employ Born–Oppenheimer molecular dynamics (BOMD) simulations at gradient-corrected DFT level with semiempirical dispersion correction to study the structural and dynamical properties of halide anions X^- (F^- , Cl^- , Br^- , and I^-) dissolved, respectively, in a water droplet (with a diameter ~ 1.8 nm) below or at the room temperature. The surface preference of heavy halide anions is confirmed by the BOMD simulations. In addition, we find that Cl^- appears to exhibit no strong tendency of either surface or bulk preference, a phenomenon, to our knowledge, not previously reported in the literature. The radial distribution functions (RDFs) of $X-O$, $X-H$, and $O-O$ and the distribution of primary bond angles are computed to show characteristics of water molecules around the halide anion and the influence of dissolved anions to the hydrogen-bonding network of water. Hydration shells, coordination number, structure of hydrated complex cores are also determined for the halide anions in the water droplet, which turn out to be different from those in aqueous solution. Additionally, diffusive property of the halide ions, residence time of water in the first hydration shell, and the lifetime of $H\cdots X$ bond are computed to gain additional insights into dynamics of the halide ions and ion/water interaction.

COMPUTATION METHODS

In the BOMD simulation, the water droplet comprises 124 water molecules and 1 halide anion. The spatial dimension of the simulation supercell is about $30 \times 30 \times 30 \text{ \AA}$, which is large enough to neglect interaction among adjacent periodic images of the droplet. To ensure equilibrium for the droplet/ion

system, two drastically different initial positions for the ion are considered for each droplet/ion system. As illustrated in Figure 1, ions are initially placed either near the surface region ($R \approx$

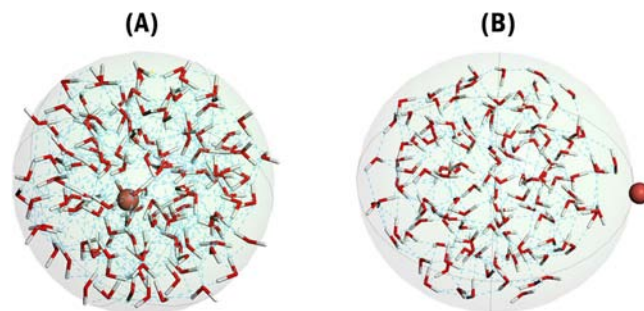


Figure 1. Initial positions of the halide anion in the water droplet: (A) in the interior region ($R = 0.2$ nm) and (B) outside the surface region ($R = 0.95$ nm), where R denotes the distance of the anion from the center of mass of the water droplet. Red: O; Gray: H.

0.95 nm) or in the interior region ($R \approx 0.2$ nm), where R denotes the distance of the ion from the center of mass of the water droplet. The system is fully relaxed before the BOMD simulation. Specifically, the Becke–Lee–Yang–Parr (BLYP) exchange–correlation functional is selected for the relaxation and BOMD simulations.^{34,35} Recently, Codorniu-Hernandez and Kusalik³⁶ have shown from their first-principle MD simulation of mobility of the hydroxyl radical in aqueous solution that the BLYP functional gives very similar results (e.g., radial distribution functions) as the functional HCTH/120.³⁷ The latter is known to describe water properties more accurately.^{37–39} The neutralizing background charge is included for the Ewald summation of electrostatic energy to compensate the net charge of the solutions. A combination of Gaussian DZVP basis set⁴⁰ and auxiliary plane waves (with an energy cutoff of 280 Ry) for expanding electron density, together with the Goedecker–Teter–Hutter (GTH) norm-conserved pseudopotentials^{41,42} for treating core electrons, is adopted for the DFT calculations. Grimme’s dispersion correction method^{43,44} is employed to combine with the BLYP functional, which would give an overall improvement of the properties of liquid water.⁴⁵ Here, we selected the BLYP-D functional because the freezing point of BLYP-D water has been recently computed.^{46a}

All the BOMD trajectories are generated in the constant volume and constant temperature (NVT) ensemble, with the Nosé–Hoover chain method for controlling the temperature of system. The time step of 1.0 fs is used, which has been proven to achieve sufficient energy conservation for the water systems considered in previous BOMD simulations.⁴⁷ The total simulation time for each system ranges from 85 to 205 ps, assuring that the ions can reach their preferable positions. All the BOMD simulations are performed using the QUICKSTEP module implemented in the CP2K package.^{48,49} Additionally, for structural analysis, the final structures of hydrated complex core of halide ions are further optimized at the MP2/6-311G(d,p) level of theory, using the GAUSSIAN 09 package.⁵⁰

Previous first-principle simulations⁴⁶ of coexisting two-phase ice/water systems indicate that the BLYP-D functional tends to overestimate the freezing point of bulk water, and the computed freezing point is about 360 K. In this study, we therefore consider two different temperatures for the BOMD simulations: (1) 300 K, which is about 60 K undercooling from

the computed freezing point (~ 360 K), and (2) 380 K, which represents room temperature.

RESULTS AND DISCUSSION

Dynamic Properties of Halide Ions. Surface Preference.

In previous experiments, it has been reported that at the room temperature the concentration enhancement near the surface arises with the size of halide anions ($\text{Cl}^- < \text{Br}^- < \text{I}^-$).^{1,5–7} The thermodynamic confirmation of such surface enhancement has been demonstrated by the depth of free energy minimum at the location of the droplet surface from the classical MD simulation.³ Interestingly, even under a supercooled temperature, BOMD trajectories of the halide ions in the water droplet (Movies S1–S10) show the surface preference of two heavy halide ions (Br^- and I^-). Taking F^- and Br^- as two extreme cases, typical snapshots of the ion solvation in the water droplet near the late stage of BOMD simulation are displayed in Figure 2. To characterize the surface region, we calculate density

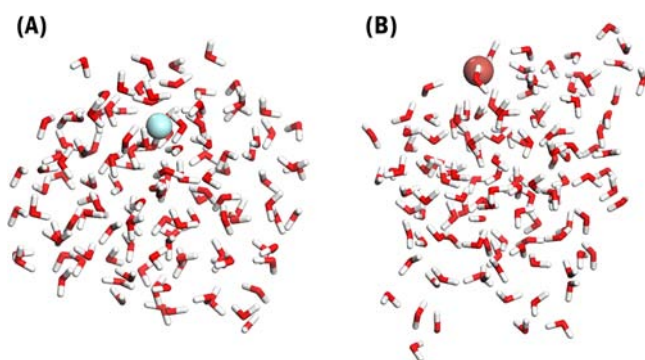


Figure 2. Snapshots of the anion in the water droplet (300 K) for (A) F^- (blue sphere) and (B) Br^- (orange sphere) at 85 ps of the BOMD simulation, respectively.

profiles of oxygen sites as a function of the radial distance from the center of mass (COM) of water molecules. As shown in Figure 3, the region beyond 7 Å from the center of mass could be viewed as the surface region (dotted-dashed line in Figure 3A,B). And the density plot of halide ion (black solid line in Figure 3B) clearly indicates the surface preference of Br^- and I^- but not for F^- . In Figure 3A, the position of halide ions (R) with respect to the COM of the water droplet (excluding the mass of the halide ion) is plotted as a function of time. When the halide ion is initially placed in the interior region (red curve in Figure 3A), one can see that in the course of BOMD simulations, Br^- and I^- are driven gradually toward the surface, while F^- stays predominately inside the water droplet. Contrary to previous classical MD simulations with polarizable models,^{3,14} our BOMD simulations show that unlike Br^- and I^- , Cl^- does not have a strong tendency to stay in the outer layer of interfacial region of the water droplet (Figure 4).

Movies S1 – S10 demonstrate that the surface region constantly deforms due to the thermodynamic fluctuations. When the ion is initially placed outside the droplet (green curves in Figure 3A and Movies S7 and S9), heavy halide ions (Br^- and I^-) remain in the surface region of the droplet. In stark contrast, the F^- ion returns to the interior region of the droplet (Movie S1). For either Br^- and I^- or F^- , both red and green curves converge to either the surface or the interior region, as shown in Figure 3B, indicating that the most favorable region for halide ions is independent of the initial

location of the ions. To summarize, even at the deeply supercooled temperature, the surface enhancement for heavy halide ions in water is confirmed from the BOMD simulations.

On the other hand, the two curves for Cl^- shown in Figure 4A demonstrate that the Cl^- ion can be, from time to time, inside or outside the interior region. In other words, the Cl^- ion appears not showing strong tendency of either surface or bulk preference at the supercooled temperature. The density profiles of the Cl^- ion also support the “itinerant” nature of the ion, which exhibit a much broader span from interior to outside the surface region (marked by the vertical dotted-dashed line). Even at the higher temperature (380 K), the density profiles (Figure 4B) show notably broader span, and the time-dependent R (Figure 4A) values exhibit higher number of crossover through the surface region compared to that at the supercooled temperature.

Self-Diffusion Coefficients of Halide Ions. Next, the dynamical and structural properties of halide ions in the droplet are computed based on the BOMD trajectories beyond 15 ps. The self-diffusion coefficient (D) can be evaluated from the mean square displacement (Figure S1), using the Einstein’s diffusion equation:

$$\langle |r(t) - r(0)|^2 \rangle = 6Dt \quad (1)$$

As shown in Table 1, the computed diffusion coefficient of the halide ions in the water droplet (at 300 K) is much smaller than the computed diffusion coefficient of water molecules (D_w) themselves in the droplet ($D_w = 1.2 \times 10^{-5}$ cm²/s). The size effect of the droplet besides the supercooled condition slows the dynamics of both halide ion and water molecules in the droplet. For example, D of Cl^- is 3.4×10^{-6} cm²/s at 300 K (see Table 1), whereas typical experiment diffusion data⁵¹ for sodium chloride in bulk solutions at the room temperature is $\sim 2 \times 10^{-5}$ cm²/s. When temperature rises to 380 K, D of Cl^- increases as well (7×10^{-6} cm²/s). Furthermore, diffusion coefficients of halide ions computed from the present simulation are in the order of $\text{F}^- \sim \text{Cl}^- < \text{Br}^- < \text{I}^-$ (see Table 1). Assuming this order is reversely correlated with the interaction between halide ions and water molecules, the smaller diffusion coefficient of Cl^- (compared to that of Br^- or I^- ion) would reflect relatively stronger interaction between Cl^- and water, which would lead to relatively longer resident time for the Cl^- ion to stay inside the water droplet than that for Br^- or I^- . Indeed, our BOMD simulations suggest that the stronger water– Cl^- interaction can be manifested by the relatively longer lifetime of water–Cl bonds compared to the water–Br or water–I bonds (see Table 1). Movies S4, S8, and S10 and Figures 3A and 4A demonstrate that the time required for the ion from interior to reach the surface region under supercooled condition follows the order: $\text{Br}^- < \text{I}^- < \text{Cl}^-$. As shown in Figures 3A and 4A (red curves), Br^- reaches the surface region ($R > 0.7$ nm) after ~ 30 ps simulation, whereas I^- takes ~ 90 ps, and Cl^- (at 300 K) takes more than 120 ps. The larger size of the I^- renders the ion more difficult to disrupt the hydrogen-bonding network of water, leading to longer time (to reach the surface) than Br^- . In the following subsection, we will analyze the structure of hydration shells surrounding the halide ions. Besides the interaction between a halide ion and water, the structure of hydration shells is another important factor that is relevant to the interior or surface preference behavior for the halide ions.

Structures of Hydration Shells Surrounding Halide Ions. Hydrating and Nonhydrating Water. Water molecules

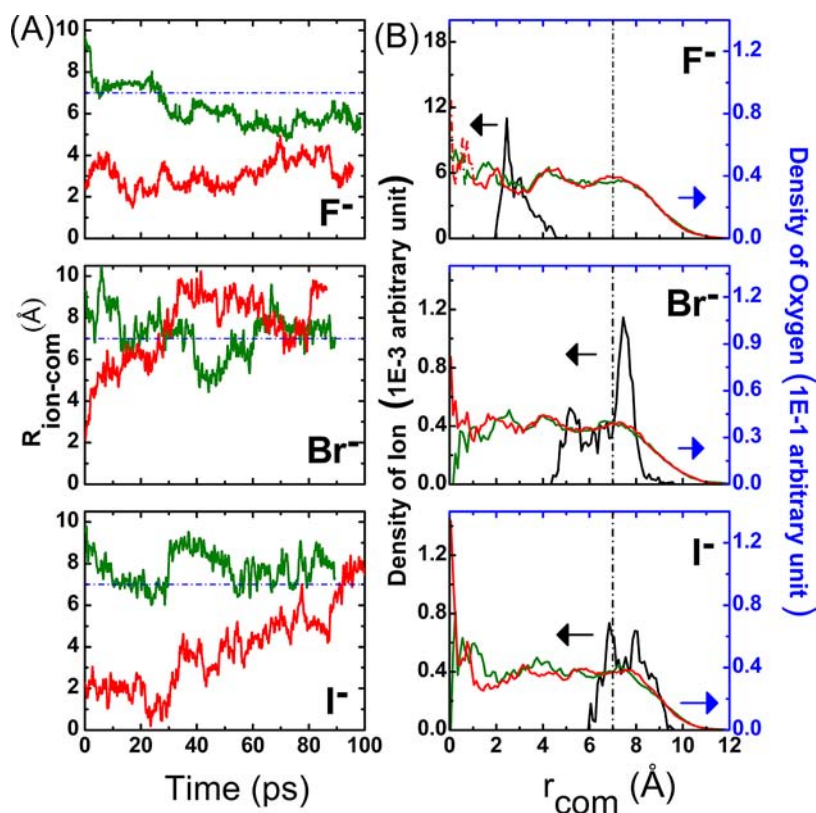


Figure 3. (A) The distance (R) between halide ion and the COM of water droplet (at 300 K) versus the time. Red curves represent time-dependent position of ions, starting initially from the interior region, while green curves represent time-dependent position of ions, starting initially outside the surface region. The blue dashed lines refer to a division between the surface and interior regions of the water droplet. (B) Density profiles of oxygen site of water droplet and halide ions at 300 K. The first 20 ps simulation is excluded from the statistical average.

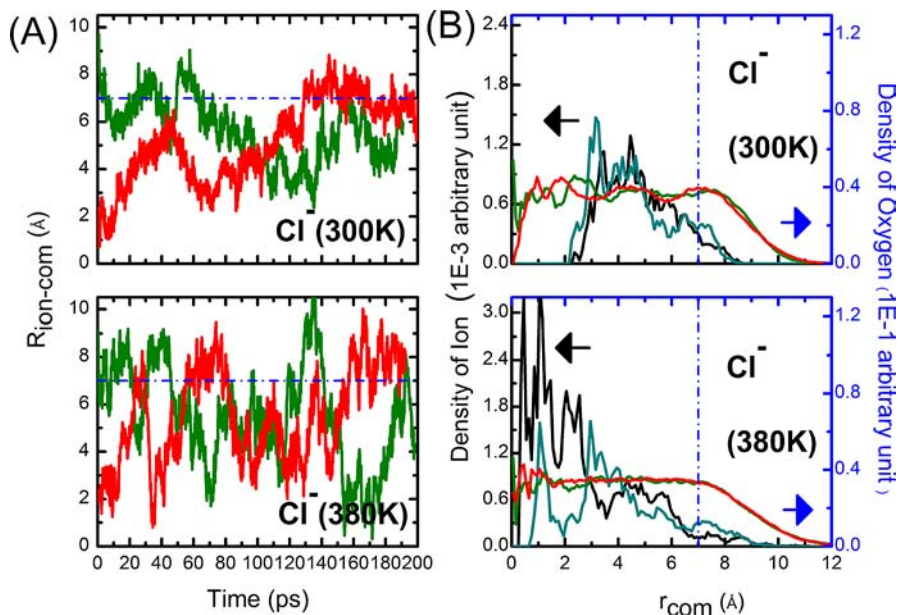


Figure 4. (A) Same as Figure 3A but for the Cl^- ion and water droplet at 300 K (upper panel) and 380 K (lower panel). (B) Density profiles of oxygen site of water droplet and halide ions at 300 K (upper panel) and 380 K (lower panel). The first 20 ps simulation is excluded from the statistical average. The cyan and black density profiles refer to the Cl^- ion whose initial position is located inside and outside the water droplet, respectively.

surrounding the halide ions can be classified into discrete hydration shells. The first and second hydration shells of the halide ions can be clearly distinguished by the first two minima in the radial distribution functions (RDFs) of the O atoms of

water molecules from the halide ions (see Figure 5A). The radii of the first and second hydration shells as well as the average numbers of water molecules in the hydration shells, obtained by integrating RDFs, increase with the size of ions (see Table 1).

Table 1. Summary of Structural and Dynamic Characteristics of Different Halide Ions in Water Droplet (300 K)^a

			first hydration shell (S1)			second hydration shell (S2)		hydrated complex core				
			R_{S1} (Å)	N_{S1}	τ (ps)	R_{S2} (Å)	N_{S2}	R_{HX} (Å)	N_h	ΔN_w	τ^* (ps)	E_b (kcal/mol)
F ⁻	1.33	3.5	3.35	5.8	6.26	5.42	18.3	2.45	5.2	0.6	5.54	27.4
Cl ⁻	1.81	3.4	3.85	7.0/7.3	3.29/3.27	6.00	18.3/19.7	2.95	5.9/6.1	1.1/1.2	2.55/2.36	14.4
Br ⁻	1.96	6.4	4.05	6.4	3.00	6.07	13.2	3.05	5.4	1.0	1.82	13.7
I ⁻	2.20	7.9	4.25	6.5	3.26	6.42	13.9	3.34	5.7	0.8	1.76	11.0

^aIonic radii⁵² and diffusion coefficient (D) of halide ions, radius (R_{S1} and R_{S2}) of first and second hydration shell, average number of water molecules or oxygen atoms (N_{S1} , N_{S2}) in the shell, average residence time of water (τ), bond length between ion and closest hydration (R_{HX}), coordination number (N_h) defined as the number of hydrogen atoms in the first shell, average number of nonhydrated water ($\Delta N_w = N_{S1} - N_h$), lifetime of H \cdots X bond (τ^*), binding energy (E_b) for single pair of halide anion and water molecule in the gas phase. Properties for Cl⁻ are computed based on both trajectories, one with initial position of Cl⁻ being located outside and another being inside the water droplet.

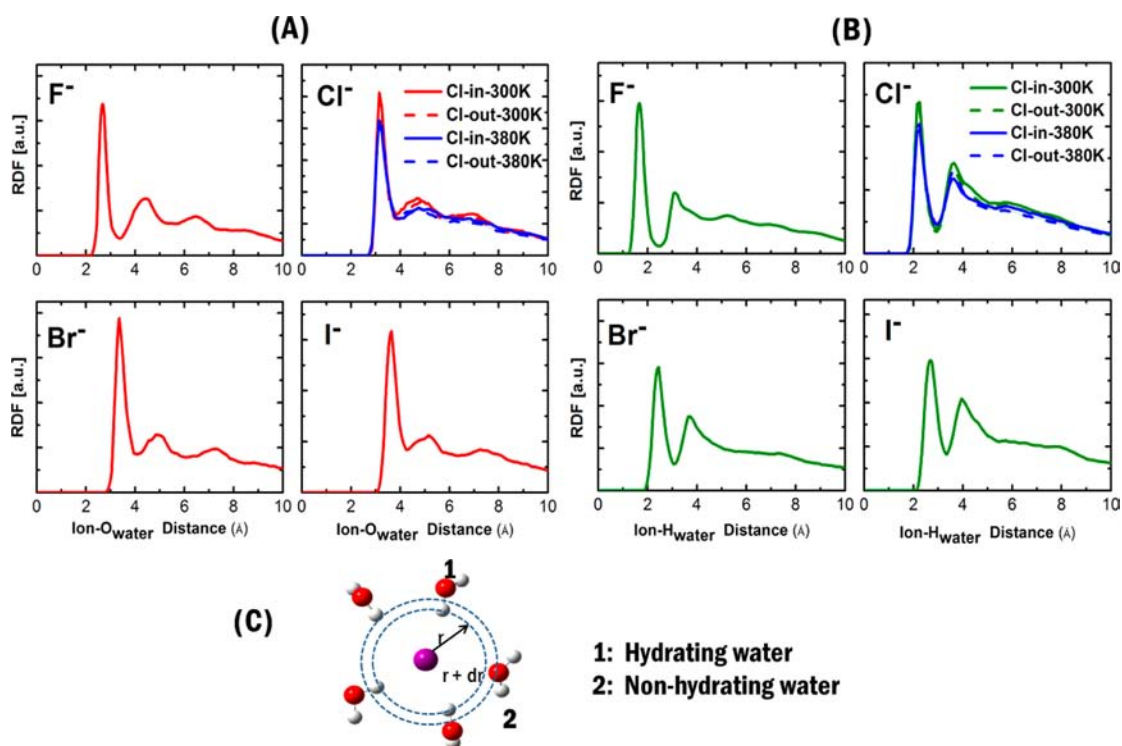


Figure 5. RDFs of (A) O atoms surrounding the halide ions and (B) H atoms surround the halide ions. (C) A schematic diagram of hydrating and nonhydrating water in the first hydration shell.

The number of water molecules in the first hydration shell of the heavy halide ions (6.4 for Br⁻ and 6.5 for I⁻) in our BOMD simulation is less than that computed from previous classical MD ($N_{Br^-} = 7.5$, $N_{I^-} = 7.9$)⁵³ or Car-Parrinello MD (CPMD) ($N_{Br^-} = 6.5$, $N_{I^-} = 8.5$)³⁰ simulations in bulk water, suggesting that the solvation structure of the heavy halide ions on the surface of a droplet differs from that in the bulk solution. The large difference in N_{Br^-} and N_{I^-} of the bulk solution between the classical MD and CPMD requires further investigation.

We also find that although the radius of second hydration shell increases with the size of the ions, the average number of water molecules in the second hydration shell shows an unexpected decrease with the size, indicating an incomplete spherical shape of the second hydration shell of the heavy ions at the surface region. According to the computed RDFs, Br⁻ and I⁻ ions are located in the surface layer of the droplet, and the F⁻ ion is located in the interior region of the water droplet,

while the Cl⁻ ion can be located in either region from time to time.

Due to negative charges of halide ions, one of the two O–H bonds of every water molecule in the first hydration shell tends to point toward the ion and form an H \cdots X bond. Those water molecules adopting such orientation are viewed as the ‘hydrating water’. Otherwise, those water molecules with no O–H bond pointing toward the halide ion are viewed as ‘nonhydrating water’ (see Figure 5C for definition). In Figure 5B, the RDFs of H atoms (H-ion RDFs) surrounding the halide ions show that the H \cdots X bonds are clearly formed in all the first hydration shell of every halide ion. The position of the first peak of H-ion RDFs refers to the length of H \cdots X bond: $R_{HX} = 1.70, 2.20, 2.45,$ and 2.67 Å for X = F⁻, Cl⁻, Br⁻, and I⁻, respectively. The average coordination number N_h of the ions can be obtained by integrating the H-ion RDFs from 0 to the first minimum (see Table 1). Note that the coordination number of the halide ions is less than the average number of

water molecules (or oxygen atoms) in the first hydration shells obtained from the O-ion RDF, indicating that not all the water molecules adopting the orientation of the 'hydrating water'. Furthermore, among the four halide ions, Cl^- , Br^- , and I^- entail more nonhydrating water molecules in their first hydration shell, compared to F^- . On average, the percentage of nonhydrating water molecules in the first hydration shell of Cl^- , Br^- , and I^- is 16%, 16% and 12%, respectively. In contrast, only 10% water molecules in the first hydration shell of F^- are 'nonhydrating'. Because the interaction between 'nonhydrating water' and halide ion is much weaker than that of the 'hydrating water', the 'nonhydrating water' molecules likely interact stronger with other water molecules and thus are easier to leave from the first hydration shell. And it is worthy of mentioning that raising the temperature to 380 K (room temperature in BLYP-based BOMD) does not significantly change the hydration structure of Cl^- .

To gain more insights into the 'hydrating water' and 'nonhydrating water', the angular distribution functions are computed to describe the microstructure of the first hydration shells of halide ions. The definition of two primary angles (θ and φ) is illustrated in Figure 6A,C, respectively. Here, the H...

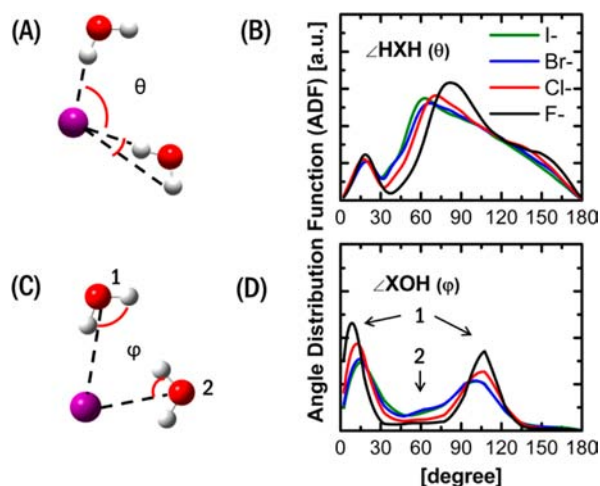


Figure 6. Definition (A and C) and angular distribution function (B and D) of the $\text{H}\cdots\text{X}\cdots\text{H}$ angle (θ) (where the two H belong to the same water molecule or two different water molecules) and $\text{X}\cdots\text{O}-\text{H}$ angle (φ) (the angle between the $\text{O}-\text{H}$ bond and the $\text{X}\cdots\text{O}$ line).

$\text{X}\cdots\text{H}$ angle (θ) (where the two H belong to the same water molecule or two different water molecules) can be used to describe the first hydration shell, while the $\text{X}\cdots\text{O}-\text{H}$ angle (φ) can illustrate whether the ion-water $\text{H}\cdots\text{X}$ bonds are well formed. The distributions of $\text{H}\cdots\text{X}\cdots\text{H}$ (θ) and $\text{X}\cdots\text{O}-\text{H}$ angles (φ) are shown in Figure 6B,D, respectively. Significant difference in the position of the primary peak for F^- ($\theta \sim 90^\circ$) and other three halide ions ($\theta \sim 60-75^\circ$) can be seen in the distribution of the $\text{H}\cdots\text{X}\cdots\text{H}$ angles. The larger θ for F^- is due to the smaller radius of F^- ion, which makes the $\text{O}\cdots\text{F}^-$ distance shorter, thereby increasing the repulsive interaction between two adjacently coordinated water molecules. From Cl^- to I^- , the θ value decreases as the distance between the ion and the nearest O atom increases. Figure 6D exhibits two major peaks, one at smaller φ ($10-15^\circ$) and another at larger φ ($100-105^\circ$), suggesting the hydrogen bond between ion and water molecule (water 1 in Figure 6C) is well formed. However, minor peaks at $\varphi \sim 60^\circ$ (Figure 6D) can be seen for

Br^- and I^- (blue and green lines), suggesting that existence of nonhydrating water molecules (as water 2 shown in Figure 6C) in the first hydration shell of Br^- and I^- . But this type of configuration rarely appears in the first hydration shell of F^- and Cl^- .

Complex Core of Hydrated Halide. Based on the average coordination number N_b , probabilities of hydrated complex with different local structures are computed in the production run, as shown in the histogram in Figure 7. One can see that

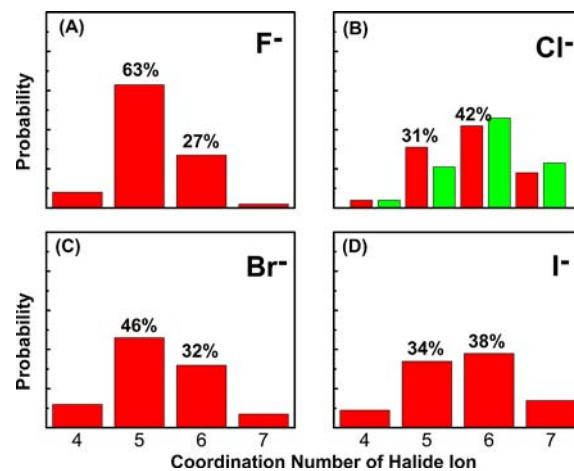


Figure 7. Histogram of probabilities of different hydrated complexes computed based on the production trajectories. Properties for Cl^- are based on both trajectories which initial position is located inside (green) and outside (red) the water droplet.

the $\text{F}(\text{H}_2\text{O})_n^-$ complex is predominantly five-fold coordinated ($n = 5$). However, for larger anions (Cl^- , Br^- , and I^-), five- and six-fold coordination complexes exhibit similar probability. To understand the microstructure of such hydrated complex core of halide ions, we also perform *ab initio* calculations for the $\text{F}(\text{H}_2\text{O})_5^-$, $\text{Cl}(\text{H}_2\text{O})_5^-$, $\text{Cl}(\text{H}_2\text{O})_6^-$, $\text{Br}(\text{H}_2\text{O})_5^-$, $\text{Br}(\text{H}_2\text{O})_6^-$, $\text{I}(\text{H}_2\text{O})_5^-$, and $\text{I}(\text{H}_2\text{O})_6^-$ complexes in the gas phase, based on the MP2/6-311G(d,p) and DFT levels of theory. Starting with halide water cluster geometries reported previously,⁵⁴ the optimized structures are displayed in Figure 8. The gas-phase structural optimization indicates that the $\text{F}(\text{H}_2\text{O})_5^-$ complex exhibits a square pyramid structure with F^- being located at the center of a bottom square formed by water molecules (Figure 8A). In contrast, the $\text{X}(\text{H}_2\text{O})_6^-$ ($\text{X} = \text{Cl}, \text{Br}$, and I) complexes exhibit various sandwich-like structures, in which six water molecules form either two opposing triangles or a square-line pair while X being located at the center between the two parts (Figure 8B-D). Likewise, the $\text{X}(\text{H}_2\text{O})_5^-$ complex shows similar structure as $\text{X}(\text{H}_2\text{O})_6^-$ but without one water in the upper part of the sandwich structure. The corresponding structural parameters (e.g., $\text{H}\cdots\text{X}$ bond lengths and $\text{H}\cdots\text{X}\cdots\text{H}$ angle) are shown in Table S2. All the structures of the gas-phase hydrated halide complex cores exhibit similar angle parameters as described by the angular distribution functions (see Figure 6).

Interaction between the halide ion and a neighbor water molecule within the hydrated complex core is weakened with increasing the $\text{H}\cdots\text{X}$ distance. Indeed, the binding energy (E_b) between an halide anion and a water molecule in the gas phase are in order of $E_b(\text{F}^-) > E_b(\text{Cl}^-) > E_b(\text{Br}^-) > E_b(\text{I}^-)$, as listed in Table 1. As the F^- ion has the smallest radius, its binding energy (~ 27 kcal/mol) is notably greater than that of other

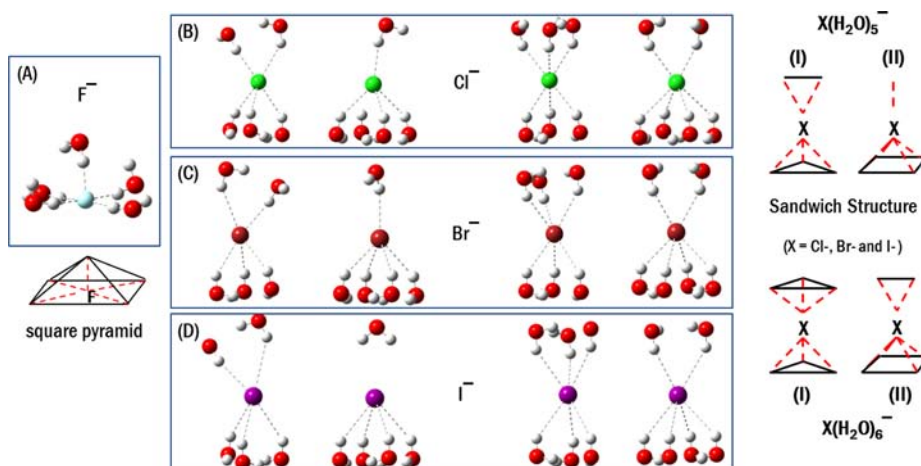


Figure 8. Geometries of gas-phase (A) $F(H_2O)_5^-$, (B) $Cl(H_2O)_5^-$ and $Cl(H_2O)_6^-$, (C) $Br(H_2O)_5^-$ and $Br(H_2O)_6^-$, and (D) $I(H_2O)_5^-$ and $I(H_2O)_6^-$ complexes, on basis of the *ab initio* optimization at MP2/6-311G(d,p) level. Schematic illustrations of various sandwich structures are given in the right panel.

three halide ions (11–14 kcal/mol). It is worthy of mentioning that the water molecule above the I^- in $I(H_2O)_5^-$ (II) complex becomes a nonhydrating water due to relatively weak interaction between I^- and water. And note that the hydrogen-bonding energy between two water molecules (calculated at the same level of theory) is 7.0 kcal/mol. Hence, the much stronger water– F^- interaction renders the F^- ion fully hydrated. On the other hand, the relatively weaker binding energies for Cl^- , Br^- , and I^- ions suggest that the formation of fully hydrated ions may be thermodynamically unfavorable due to the higher free-energy penalty of breaking hydrogen network of water. Therefore, the larger ions tend to reside near the surface region to offset some of the free-energy penalty. In agreement with previous theoretical study,⁵⁵ there is no significant binding energy difference between five- and six-fold coordinated complexes for Cl^- , Br^- , and I^- ions as listed in Table S1. This result is also consistent with the computation results that the two coordination numbers (5 and 6) exhibit similar probabilities in the BOMD simulation (Figure 7B–D). The charge distribution of hydrated-complex core is also computed by using natural bond orbital analysis (see Table S1). The amount of charge transfer between halide anions and water molecules decreases from F^- to I^- , consistent with corresponding binding energy decrement.

Hydration Asymmetry of Halide Ions. In Figure 9, we plot the distance between halide ion and the center of mass (COM) of surrounding water molecules versus increasing size of water cluster. The degree of solvation asymmetry of halide anion in the water droplet can be measured by the height profile of the curve versus the number of water molecules. Note that the curves have been moved upward from F^- to I^- , indicating increased anisotropy with the size of halide anions. For F^- , the distance from ion to the COM of surrounding waters only shows slightly change when extending the size of solvating water clusters from the first hydration shell, suggesting the bulk preference of F^- in the water droplet. However, for Br^- and I^- , the curves reach the minimum at $N = 6$ (the size of their first hydration shell) and then raises up with increasing water cluster size, consistent with surface enhancement behavior of heavy halide ions (Br^- and I^-) and their incomplete spherical shape of the second hydration shell. Unlike F^- or Br^-/I^- , the curve for Cl^- reaches minima at $N = 8$ and 16 (close to the size of its first

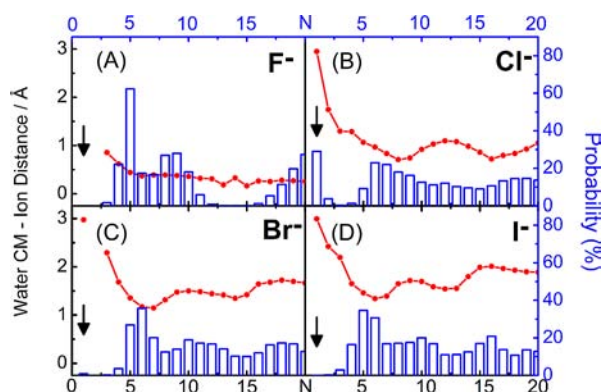


Figure 9. With different distances from the ion to the COM of water cluster (starting from 1.0 Å), various solvating water clusters are assigned. Solvation anisotropy plot for halide water clusters containing N water molecules is marked in red dots. Blue histogram shows probability of the appearance of each water cluster. Due to similar solvation behavior of Cl^- at 300 and 380 K, similar distance curve and probability distribution are obtained. Trajectory of water droplet with Cl^- being initially placed at the surface region (at 300 K) is used for the plot. Black arrows refer to the probability of $N = 1$ for the four anions.

and second hydration shells) due to the unique solvation behavior. We also calculate the probabilities of each solvating water cluster around the halide anion. As can be seen in Figure 9, the unusually high probability of $N = 1$ for Cl^- (marked by black arrow) signifies flexible solvating water molecules in the first hydration shell.

Hydrogen-Bonding Network Surrounding Halide Ions. It is known that liquid water entails a strong hydrogen-bonding network. However, the introduction of halide ions can locally distort such a hydrogen network. To provide a description of the microstructure of water surrounding the halide ions, we compute O–O pair correlation functions (PCFs) for water molecules in the first hydration shell (S1–S1), the second hydration shell (S2–S2), and bulk-like water (bulk–bulk) as well as the intershell contacts (S1–S2 and S2–bulk), respectively. All the PCFs are normalized (see Figure 10). For water molecules in the bulk-like region (water molecules beyond the second hydration shell of the halide ions), the primary peak (black lines) at $r = 2.75$ Å characterizes the

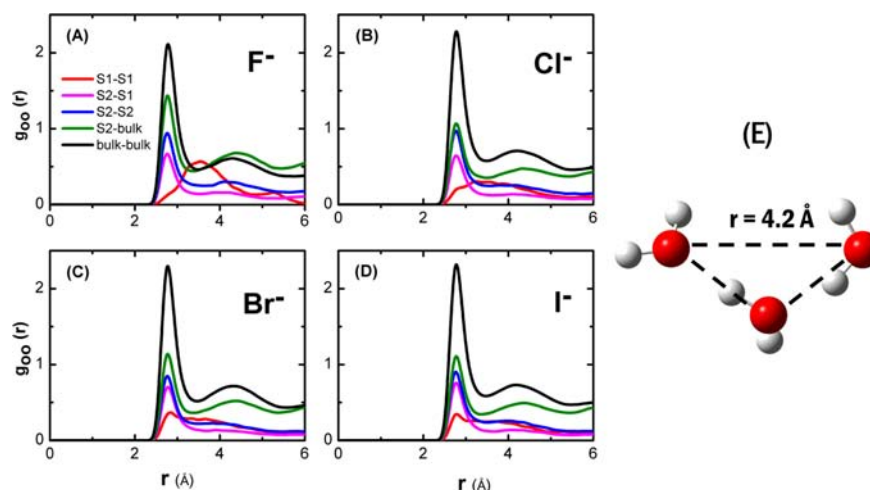


Figure 10. Oxygen–oxygen PCF within a hydration shell, between two hydration shells, or in bulk water.

intermolecular hydrogen bonds among water, and the broader peak at $r \approx 4.2$ Å characterizes the water pair, both hydrogen bonded to a third water molecule (see Figure 10E). The first peaks at $r = 2.75$ Å are very weak in the S1–S1 PCFs of F^- and Cl^- (red lines in Figure 10A,B), suggesting that the hydrogen-bonding network is not well formed in the first hydration shell. For F^- , the first peak completely vanishes, indicating that the water– F^- interaction is strong enough to displace a higher number of water–water hydrogen bonds. The first peaks of the S1–S1 PCFs for Br^- and I^- ions (red lines in Figure 10C,D), although decrease significantly compared to that of the bulk water, are still more distinguishable than those of F^- and Cl^- ions. This result suggests that the interaction between Br^- (or I^-) and water is not so strong such that the water molecules can still form hydrogen bonds in the first hydration shell. In contrast to S1–S1 PCFs, the peaks at $r = 2.75$ Å are much higher in S1–S2 (pink lines) and S2–S2 (blue lines) PCFs, demonstrating that the hydrogen bonds are preserved in the second hydration shell. In S2–bulk PCFs (green lines), the first and second peaks are clearly seen, suggesting that the hydrogen-bonding network is retained in the region.

Dynamical Properties of Hydration Shells. Lastly, we study dynamical stability of the hydration shells surrounding the halide ions by computing the residence time of water molecules in the hydration shell and average lifetime of $H\cdots X$ hydrogen bonds. These results can provide better understanding of possible surface preference behavior for the hydrated halide ions. Based on trajectories of the BOMD simulation, the computed average residence time (τ) of water molecules in certain hydration shell is listed in Table 1. It can be seen that the average residence time of water molecules in the first hydration shell decreases rapidly with increasing the ion size. The correlation function $C(t)$ of the resident time is given by

$$\langle C(t) \rangle = \left\langle \frac{1}{N_{s1}} \sum_{i=1}^{N_{s1}} [h_i(0)h_i(t)] \right\rangle \quad (2)$$

where N_{s1} is the hydration number, $h_i(t)$ is 1 or 0 for a water molecule inside or outside the assigned hydration shell at time t . Computed $C(t)$ (see Figure S2) also indicates that water molecules around F^- have the longest residence time in the first hydration shell due to the strongest interaction between water molecules and F^- . In contrast, water molecules around Cl^- ,

Br^- , and I^- ions exhibit more or less the same residence time, about a half of the residence time for the F^- ion. The average lifetime of $H\cdots X$ hydrogen bond (τ^*) is computed using the similar method as for τ . As shown in Table 1, $\tau^*(F^-) > \tau^*(Cl^-) > \tau^*(Br^-) \approx \tau^*(I^-)$. The magnitude of τ^* (ps) is close to the measured residence time ($\sim 10^{-10}$ s) for halide anions in aqueous solution by quasi-elastic neutron scattering.⁵⁶ The decay rate of the correlation function of the lifetime for different halide ions also supports this result (see Figure S3). In general, τ^* is slightly shorter than τ since the orientation fluctuations of water molecules in the first shell tend to contribute more significantly to the breaking of hydrogen bonds, such as the transition between five- and six-fold complexes. In summary, both the residence time of water molecules and the lifetime of $H\cdots X$ bonds show that F^- possesses a highly stable first hydration shell, which can prevent the F^- ion from diffusing into the surface region of water droplets. However, the first hydration shell is relatively less stable for heavy halide ions, where the high exchange rates of water molecules in the hydration shells render the ions easier to migrate into the surface region of the droplet.

CONCLUSION

We have performed first-principles BOMD simulations to study structural and dynamical properties of hydrated F^- , Cl^- , Br^- , and I^- ions in a water nanodroplet, respectively. In agreement with previous experimental measurements, the heavy halide anions (Br^- and I^-) tend to be located near the surface region of the supercooled water droplet, whereas F^- still exhibits interior solvation in the supercooled water droplet. However, Cl^- appears to exhibit no strong tendency of either surface or bulk preference, either at the supercooled or room temperature. This phenomenon has not previously reported in literature. Moreover, the rate for the ions to move from the interior to the surface region (under supercooled condition) follows the order: $Cl^- < I^- < Br^-$, which is not necessarily correlated with the size of ions.

Compared with classical MD simulation of bulk water at ambient condition, here, less water molecules are observed in the first and second hydration shells of the halide ions in the surface region. Around the halide ions, both ‘hydrating’ and ‘nonhydrating water’ can be identified. Local hydrogen-bonding network of water molecules around F^- and Cl^- ion is fully

disrupted. However, around the two larger halide ions, the local hydrogen-bonding network still survives. By counting the coordination number of the halide ions, it is found that the five-fold coordinated F^- complex is predominant while five- and six-fold Cl^- , Br^- , and I^- complexes can be both present periodically, indicating the existence of nonhydrated water molecules in the first hydration shell. Gas-phase computation at the high-level of *ab initio* theory suggests that the $F(H_2O)_5^-$ core exhibits square pyramidal structure, while the $X(H_2O)_n^-$ ($n = 5, 6$; $X = Cl, Br, I$) complexes exhibit sandwich-like structures. Furthermore, the water- F^- binding energy is much greater than the hydrogen-bonding energy of water, whereas the binding energies for Cl^- , Br^- , and I^- are much weaker. Finally, the average residence time of water molecules in the first hydration shell (τ) and the lifetime of $H\cdots X$ hydrogen bond (τ^*) are comparable, and both show that the first hydration shell of F^- ion is much more stable than that of Cl^- , Br^- , and I^- ions.

■ ASSOCIATED CONTENT

📄 Supporting Information

Movies of halide ions in a water droplet are collected, including summary of calculated binding energy (E_b) per water at different theoretical level for hydrated-complex cores and water dimer, summary of calculated geometry parameters at different theoretical level, curves of the mean square displacement versus time, residence-time correlation functions of water molecules in the first hydration shell, and lifetime correlation function of $H\cdots X$ bonds ($X = F^-, Cl^-, Br^-,$ and I^-) are collected. This material is available free of charge via the Internet at <http://pubs.acs.org>.

■ AUTHOR INFORMATION

Corresponding Author

xzeng1@unl.edu

Notes

The authors declare no competing financial interest.

■ ACKNOWLEDGMENTS

This work is supported by grants from the NSF (CBET-1066947 and CHE-1306326) and ARL (W911NF1020099), the Nebraska Research Initiative, and by the University of Nebraska Holland Computing Center.

■ REFERENCES

- (1) Brown, M. A.; D'Auria, R.; Kuo, I. F. W.; Krisch, M. J.; Starr, D. E.; Bluhm, H.; Tobias, D. J.; Hemminger, J. C. *Phys. Chem. Chem. Phys.* **2008**, *10*, 4778.
- (2) Cabarcos, O. M.; Weinheimer, C. J.; Lisy, J. M.; Xantheas, S. S. *J. Chem. Phys.* **1999**, *110*, 5.
- (3) Caleman, C.; Hub, J. S.; van Maaren, P. J.; van der Spoel, D. *Proc. Natl. Acad. Sci. U.S.A.* **2011**, *108*, 6838.
- (4) Cheng, J.; Vecitis, C. D.; Hoffmann, M. R.; Colussi, A. J. *J. Phys. Chem. B* **2006**, *110*, 25598.
- (5) Cheng, M. H.; Callahan, K. M.; Margarella, A. M.; Tobias, D. J.; Hemminger, J. C.; Bluhm, H.; Krisch, M. J. *J. Phys. Chem. C* **2012**, *116*, 4545.
- (6) Ghosal, S.; Brown, M. A.; Bluhm, H.; Krisch, M. J.; Salmeron, M.; Jungwirth, P.; Hemminger, J. C. *J. Phys. Chem. A* **2008**, *112*, 12378.
- (7) Ghosal, S.; Hemminger, J. C.; Bluhm, H.; Mun, B. S.; Hebenstreit, E. L. D.; Ketteler, G.; Ogletree, D. F.; Requejo, F. G.; Salmeron, M. *Science* **2005**, *307*, 563.
- (8) Jungwirth, P.; Tobias, D. J. *Chem Rev* **2006**, *106*, 1259.
- (9) Liu, D. F.; Ma, G.; Levering, L. M.; Allen, H. C. *J. Phys. Chem. B* **2004**, *108*, 2252.

- (10) Onorato, R. M.; Otten, D. E.; Saykally, R. J. *J. Phys. Chem. C* **2010**, *114*, 13746.
- (11) Petersen, P. B.; Johnson, J. C.; Knutsen, K. P.; Saykally, R. J. *Chem. Phys. Lett.* **2004**, *397*, 46.
- (12) Raymond, E. A.; Richmond, G. L. *J. Phys. Chem. B* **2004**, *108*, 5051.
- (13) Tobias, D. J.; Hemminger, J. C. *Science* **2008**, *319*, 1197.
- (14) Yoo, S.; Lei, Y. A.; Zeng, X. C. *J. Chem. Phys.* **2003**, *119*, 6083.
- (15) Finlaysonpitts, B. J. *Nature* **1983**, *306*, 676.
- (16) Finlaysonpitts, B. J.; Ezell, M. J.; Pitts, J. N. *Nature* **1989**, *337*, 241.
- (17) Finlaysonpitts, B. J.; Livingston, F. E.; Berko, H. N. *Nature* **1990**, *343*, 622.
- (18) Foster, K. L.; Tolbert, M. A.; George, S. M. *J. Phys. Chem. A* **1997**, *101*, 4979.
- (19) Knipping, E. M.; Lakin, M. J.; Foster, K. L.; Jungwirth, P.; Tobias, D. J.; Gerber, R. B.; Dabdub, D.; Finlayson-Pitts, B. J. *Science* **2000**, *288*, 301.
- (20) Oum, K. W.; Lakin, M. J.; DeHaan, D. O.; Brauers, T.; Finlayson-Pitts, B. J. *Science* **1998**, *279*, 74.
- (21) Hu, J. H.; Shi, Q.; Davidovits, P.; Worsnop, D. R.; Zahniser, M. S.; Kolb, C. E. *J. Phys. Chem.* **1995**, *99*, 8768.
- (22) Finlayson-Pitts, B. J. *Phys. Chem. Chem. Phys.* **2009**, *11*, 7760.
- (23) Samaras, N. N. T. *J. Phys. Chem.* **1933**, *37*, 437.
- (24) Becke, T. L. *Chem. Phys. Lett.* **2013**, *561*, 1.
- (25) Krekeler, C.; Hess, B.; Delle Site, L. *J. Chem. Phys.* **2006**, *125*, 054305.
- (26) Masia, M.; Probst, M.; Rey, R. *Chem. Phys. Lett.* **2006**, *420*, 267.
- (27) Rogers, D. M.; Beck, T. L. *J. Chem. Phys.* **2010**, *132*, 014505.
- (28) Baer, M. D.; Mundy, C. J. *J. Phys. Chem. Lett.* **2011**, *2*, 1088.
- (29) Wick, C. D.; Xantheas, S. S. *J. Phys. Chem. B* **2009**, *113*, 4141.
- (30) Guardia, E.; Skarmoutsos, I.; Masia, M. *J. Chem. Theory Comput.* **2009**, *5*, 1449.
- (31) Masia, M. *J. Chem. Phys.* **2008**, *128*, 184107.
- (32) Ishiyama, T.; Morita, A. *J. Phys. Chem. C* **2007**, *111*, 721.
- (33) Wick, C. D. *J. Chem. Phys.* **2009**, *131*, 084715.
- (34) Becke, A. D. *Phys. Rev. A* **1988**, *38*, 3098.
- (35) Lee, C. T.; Yang, W. T.; Parr, R. G. *Phys. Rev. B* **1988**, *37*, 785.
- (36) Codorniu-Hernandez, E.; Kusalik, P. G. *J. Am. Chem. Soc.* **2012**, *134*, 532.
- (37) Boese, A. D.; Doltsinis, N. L.; Handy, N. C.; Sprick, M. *J. Chem. Phys.* **2000**, *112*, 1670.
- (38) Izvekov, S.; Voth, G. A. *J. Chem. Phys.* **2005**, *123*, 044505.
- (39) Boese, A. D.; Martin, J. M. L. *J. Chem. Phys.* **2004**, *121*, 3405.
- (40) VandeVondele, J.; Hutter, J. *J. Chem. Phys.* **2007**, *127*, 114105.
- (41) Goedecker, S.; Teter, M.; Hutter, J. *Phys. Rev. B* **1996**, *54*, 1703.
- (42) Hartwigsen, C.; Goedecker, S.; Hutter, J. *Phys. Rev. B* **1998**, *58*, 3641.
- (43) Grimme, S. *J. Comput. Chem.* **2004**, *25*, 1463.
- (44) Grimme, S. *J. Comput. Chem.* **2006**, *27*, 1787.
- (45) Baer, M. D.; Mundy, C. J.; McGrath, M. J.; Kuo, I. F.; Siepmann, J. I.; Tobias, D. J. *J. Chem. Phys.* **2011**, *135*, 124712.
- (46) (a) Yoo, S.; Xantheas, S. S. *J. Chem. Phys.* **2011**, *134*, 121105. (b) Yoo, S.; Zeng, X. C.; Xantheas, S. S. *J. Chem. Phys.* **2009**, *130*, 221102.
- (47) Mares, J.; Liimatainen, H.; Laasonen, K.; Vaara, J. *J. Chem. Theory Comput.* **2011**, *7*, 2937.
- (48) VandeVondele, J.; Krack, M.; Mohamed, F.; Parrinello, M.; Chassaing, T.; Hutter, J. *Comput. Phys. Commun.* **2005**, *167*, 103.
- (49) Lippert, G.; Hutter, J.; Parrinello, M. *Mol. Phys.* **1997**, *92*, 477.
- (50) Frisch, M. J.; Trucks, G. W.; Schlegel, H. B.; Scuseria, G. E.; Robb, M. A.; Cheeseman, J. R.; Scalmani, G.; Barone, V.; Mennucci, B.; Petersson, G. A.; Nakatsuji, H.; Caricato, M.; Li, X.; Hratchian, H. P.; Izmaylov, A. F.; Bloino, J.; Zheng, G.; Sonnenberg, J. L.; Hada, M.; Ehara, M.; Toyota, K.; Fukuda, R.; Hasegawa, J.; Ishida, M.; Nakajima, T.; Honda, Y.; Kitao, O.; Nakai, H.; Vreven, T.; Montgomery, J. A., Jr.; Peralta, J. E.; Ogliaro, F.; Bearpark, M.; Heyd, J. J.; Brothers, E.; Kudin, K. N.; Staroverov, V. N.; Kobayashi, R.; Normand, J.; Raghavachari, K.; Rendell, A.; Burant, J. C.; Iyengar, S. S.; Tomasi, J.; Cossi, M.; Rega,

N.; Millam, N. J.; Klene, M.; Knox, J. E.; Cross, J. B.; Bakken, V.; Adamo, C.; Jaramillo, J.; Gomperts, R.; Stratmann, R. E.; Yazyev, O.; Austin, A. J.; Cammi, R.; Pomelli, C.; Ochterski, J. W.; Martin, R. L.; Morokuma, K.; Zakrzewski, V. G.; Voth, G. A.; Salvador, P.; Dannenberg, J. J.; Dapprich, S.; Daniels, A. D.; Farkas, Ö.; Foresman, J. B.; Ortiz, J. V.; Cioslowski, J.; Fox, D. J. *Gaussian 09*; Gaussian Inc.: Wallingford, CT, 2009.

(51) Mills, R.; Lobo, V. M. M. *Self-diffusion in electrolyte solutions: a critical examination of data compiled from the literature*; Elsevier: Amsterdam, 1989.

(52) Shannon, R. D. *Acta Crystallogr. A* **1976**, *32*, 751.

(53) Koneshan, S.; Rasaiah, J. C.; Lynden-Bell, R. M.; Lee, S. H. *J. Phys. Chem. B* **1998**, *102*, 4193.

(54) Likholyot, A.; Hovey, J. K.; Seward, T. M. *Geochim. Cosmochim. Acta* **2005**, *69*, 2949.

(55) Lee, H. M.; Kim, D.; Kim, K. S. *J. Chem. Phys.* **2002**, *116*, 5509.

(56) Salmon, P. S.; Howells, W. S.; Mills, R. *J. Phys. C: Solid State Phys.* **1987**, *20*, 5727.